sensors

Article

Cervical Tissue Hydration Level Monitoring by a Resonant Microwave Coaxial Probe

Heungjae Choi [1]*, Emilia Barker [2], Ali A Abduljabar [3], Dilly Anumba [4], and Adrian Porch [1]

[1] School of Engineering, Cardiff University, 14-17 The Parade, Cardiff, CF24 3AA, United Kingdom; ChoiH1@cardiff.ac.uk (H.C.); PorchA@cardiff.ac.uk (A.P.)
[2] School of Clinical Dentistry, University of Sheffield, 19 Claremont Crescent, Sheffield, S10 2TA, United Kingdom; emilia.barker@sheffield.ac.uk (E.B.)
[3] College of Engineering, University of Basrah, 61002, Basrah, Iraq; ali.abduljabar@uobasrah.edu.iq (A.A.)
[4] Department of Oncology and Metabolism, JW4/40, Level 4, Jessop Wing, Tree Root Walk, Sheffield, S10 2SF; d.o.c.anumba@sheffield.ac.uk (D.A.)

* Correspondence: PorchA@cardiff.ac.uk

Abstract: Cervical tissue hydration level is one of the most important parameters to monitor in the early diagnosis of pre-term birth. Electrical impedance spectroscopy-based techniques are often used but they suffer from limited accuracy. Open microwave coaxial probes have been widely used as a broadband dielectric characterization technique for human tissue samples for its versatility, but with limited accuracy due to its non-resonant nature. In this work, a resonant microwave open coaxial probe with multiple harmonic resonances is proposed as a sensing platform for tissue hydration level monitoring. Mechanical design was analyzed and verified by finite-element full 3-D electromagnetic simulation and experiments. Dominant sources of errors and the ways to mitigate them were discussed. *In vitro* experiments were carried out with human cervix samples to verify the precision and accuracy, by comparing the results to a commercial skin hydration sensor. The proposed sensor shows mean fractional frequency shift of (3.3±0.3)*10^{-4} per unit % over the entire data. This translates into an absolute frequency shift (Δf_N) of 252±23 kHz/%, 455±41 kHz/%, and 647±57 kHz/% at 2nd, 4th, and 6th harmonic resonance, respectively.

Keywords: Harmonic resonance; microwave; preterm birth; sensing; tissue hydration.

Citation: Lastname, F.; Lastname, F.; Lastname, F. Title. *Sensors* **2022**, *22*, x. https://doi.org/10.3390/xxxxx

Academic Editor: Firstname Lastname

Received: date
Accepted: date
Published: date

1. Introduction

Every year, an estimated 15 million babies are born preterm, defined as 37 completed weeks of gestation [1]; this is more than 1 in 10 babies and is rapidly rising. Spontaneous preterm birth and the relevant complications are responsible for about 1 million deaths in 2015, becoming the leading cause of death among children under 5 years of age [2]. Unfortunately, the majority of survivors end up experiencing life-long developmental delay with breathing, vision, and hearing problems [3].

Microstructural changes to the cervix such as cervical softening, shortening and dilation, are known to be common indicators of preterm birth [4]. Tissue hydration, collagen structure and tissue elasticity progressively change with cervical microstructure change as pregnancy progresses [5][6].

Tissue hydration can be measured and monitored in several direct and indirect methods: (1) Dilution techniques based on laboratory analysis of a tracer concentration in blood and urine samples [7], (2) biological impedance and conductance methods, including single frequency bioelectrical impedance analysis [8] and biological impedance spectroscopy, which measures resistance and reactance over wide range of frequencies [9][10], (3) total body electrical conductivity using a solenoid that generates a time-varying electromagnetic field and eddy currents [11]. There were some attempts in development of segmental bioelectrical impedance methods, however, their accuracy was not adequate [12]. Medical imaging techniques, such as magnetic resonance imaging (MRI) and ultrasonography, are potentially sensitive to water content in the tissue and are widely used for visualization of internal structures and finding lesions, but not for assessment of water content [13][14]. However, despite attempts to use water-selective modes in contrast MRI [15][16], in general, the imaging techniques are not suitable for quantitative evaluation of water content. Nuclear magnetic resonance analysis of microwave-dried meat samples [17] was used for fast determination of fat and water content but is not suitable for *in vivo* experiments. The same applies to optical infrared reflectance spectroscopy [18]. Optical digital imaging is easy and straightforward, but imprecise and semi-quantitative [19]. Electrical impedance spectroscopy has shown little clinical utility [20], and acoustic attenuation measurement requires tissue homogeneity and shows wide intra-subject variability [21]. Stromal differentiation using Raman spectroscopy is expensive and semi-quantitative [22].

Magnetic induction spectroscopy is another emerging technique that shows promising results in cervical tissue measurements [23]-[25]. Some commercial instruments are able to measure the water content of the skin, based on conductance measurements, such as Skicon (I.B.S. Co., Ltd, Japan), or capacitance, such as Corneometer® (Courage Khazaka electronic GmbH, Germany) and NOVA Dermal Phase Meter (Nova Technology Corporation, USA) [26]. Such corneometers are claimed to have ±3% accuracy over the measurement frequency of 0.9 – 1.2 MHz [27].

Microwave dielectric spectroscopy is a useful and powerful technique in the characterization, sensing, and monitoring of human tissue properties for its key advantages such as nondestructive, noninvasive, and label-free measurements, as well as rapid and focused power delivery capability for therapeutic applications [28]-[37]. The high dielectric constant of water produces high dielectric contrast when combined with other materials, such as human tissues, therefore making dielectric spectroscopy a strong candidate for cervix tissue hydration monitoring.

The commonly-used microwave cavity perturbation technique would provide high accuracy at a selected frequency among available dielectric characterization methods, but it requires bulky resonator and specific sample shape and volume, therefore it is not suitable for *in vivo* sensing and monitoring [38][39]. Although less accurate due to its non-resonant nature, the coaxial reflectance probe is best suited for lossy samples such as liquids and malleable samples for its contact-based sensing mechanism and broadband characteristics. Therefore, it has been a popular choice for several decades in biological tissue characterization [40]-[53]. A novel coupling technique allowed transmission measurements from one end of a half-wavelength coaxial resonator, which improved the dynamic range while allowing the evanescent field at the sample-end of the resonator [54]-[60]. Combination of high accuracy from the resonator-based perturbation mechanism, convenience of open coaxial probe and its form factor, and broadband information obtained from harmonic resonances will constitute an ideal technique for non-invasive *in vivo* cervix tissue hydration monitoring.

Design, mechanical construction, and characterization via simulation and measurement of the 2-port coaxial harmonic resonance probe and relevant factors that affects accuracy are discussed in Section 2. Section 3 includes the details of sample preparation, test procedure, and data processing routine. The results comparing the proposed technique and the commercial Corneometer® are summarized and discussed in Section 4, followed by conclusions in Section 5.

2. Probe Design and Characterization

2.1. Advantages of 2-port transmission measurement

The complex permittivity of the samples under test are measured by their perturbation of the electric field at the open end of the coaxial resonator. There are several advantages of choosing the transmission (2-port) over the reflection (1-port) technique for resonator measurements of material properties. The main advantage is that it is possible to use weak coupling, which allows much simpler conversion of loaded quality factor to unloaded quality factor without the need for careful calibration. A weak coupling also means that the coupling structure does not perturb the electromagnetic field within the resonator, therefore minimizing the impact of the coupling structures in the material properties extraction. Another huge advantage is that, similar to a resonant cavity, in the 2-port measurement technique the dielectric properties of the sample can be extracted by simple ‘relative’ measurement between *air* and *sample*. This allows us to avoid solving a complicated inverse problem (that is, calculating dielectric properties from the measured admittance) and reduce the requirement of the vector network analyzer and calibration procedure [61]-[63]**.** In other words, we can simply utilize a low-cost scalar network analyzer in extracting complex permittivity, so it is possible to design a miniaturized portable diagnostic system around the resonator.

2.2. 2-port Harmonic Resonance Coaxial Probe Design

To avoid any non-TEM modes and to ensure broadband operation, the cross-sectional dimensions of the probe should be much smaller than the wavelength**.** As shown in Figure 1, PTFE-filled RG401 (inner conductor diameter 1.63±0.03 mm, outer conductor 6.35±0.03 mm) 50 Ω coaxial cable is chosen in the design for several reasons, but mainly for its wide availability, low cost, and rigidity for cervix tissue hydration monitoring application. Both ends of the coaxial cable are cut and flattened to form half-wavelength resonator, where one end will be in touch with the sample-under-test while the opposite end will have input and output coupling ports. A small hole (e.g., radius of 2mm) is required at the outer conductor and the PTFE of the coaxial cable at port 2 location in Figure 1 (a) to allow coupling. The relationship between the length and resonant frequencies can be defined as follows [39],

$$f_N = \frac{N}{2l} \cdot \frac{c}{\sqrt{\varepsilon_r}}, \qquad (1)$$

where f_N is the harmonic resonant frequency, l is the length of the coaxial resonator, N is the harmonic number (defined to be the number of half wavelengths along the length), c is the speed of light in vacuo and ε_r is the relative permittivity of the dielectric filler material (PTFE). According to (1), a length of 300 mm gives a fundamental resonant frequency of about 350 MHz, with higher order harmonics at integer multiples of the fundamental frequency. This length allows the investigation of the dielectric properties of the target sample-under-test (i.e. water-based tissues) over RF (low *N*) and the lower microwave frequency range (high *N*).

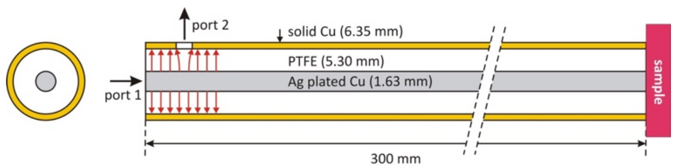

(a)

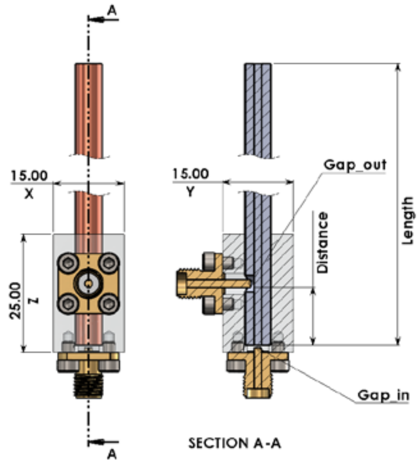

(b)

Figure 1. Mechanical construction of the 2-port coaxial harmonic resonance probe. (a) Coaxial resonator formed from an open-ended coaxial cable (RG401, with material diameters shown), and (b) 3D CAD model of the complete coaxial resonant probe with break view in the length of coaxial cable. Cross-section A-A shows the detailed coupling structure inside the aluminum fixture that hosts two SMA connectors and the RG401 cable (All units in mm).

Capacitive coupling to the electric field (E-field), as shown schematically with the red arrows in Fig. 1 (a), is made at one end of the cable using a short, extruded inner conductor of an SMA connector, and the sample is placed at the other end. As illustrated in Figure 1 (b), a rectangular aluminum fixture (15x15x25 mm^3) is used to hold the coaxial cable and two coupling ports of the SMA connectors. Since the coaxial cable is open circuit at each end, the E-field in each resonant mode is maximum at both ends, yielding effective microwave coupling that increases with increasing frequency, and effective E-field coupling to the sample for assessment of its dielectric properties. To achieve weak coupling, as discussed in the previous section, the gap between the inner conductor of the coaxial resonator and each coupling port (*Gap_in* and *Gap_out*) were adjusted so that both port 1 and 2 have symmetric coupling strength and produce insertion loss (S_{21}) of 30 dB at the fundamental resonant frequency. This requires *Gap_in* and *Gap_out* to be about 1 mm. The distance between the two ports (*Distance*) is chosen to be 13mm so that there is little direct coupling between two ports. Due to this unique coupling structure, one of the harmonic resonances (e.g., N = 10) is diminished when the distance equates to the quarter wavelength of that specific harmonic frequency. This will be further investigated with the aid of 3D finite element simulation in the next section.

2.3. Simulation and Characterization

The E-field magnitude along the length and inside of the coaxial resonant probe for the first four modes (N is the mode number) calculated and illustrated in Figure 2 based on the theoretical expression for electric field, i.e. simple sinusoids of degreasing wavelength (Scale: red is high, purple is low). Both ends of the coaxial cable are assumed to be an open circuit, hence Figure 2 shows maximum E-field at these ends

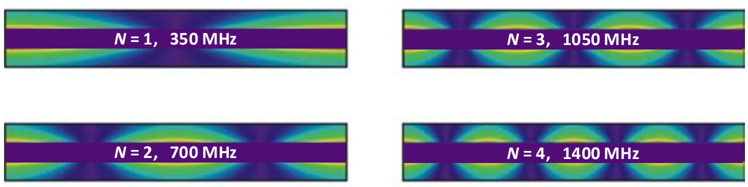

Figure 2. Calculated E-field distribution of the first four modes within an open-ended coaxial resonator (Scale: red is high, purple is low).

The probe in full 3D geometry is also simulated in COMSOL Multiphysics by using the model illustrated in Figure 1 and the E-field distribution is plotted at 350 MHz (*N*=1) in Figure 3 (a) and (b), and at 1400 MHz (*N*=4) in Figure 3 (c), respectively. The model is a one-to-one replica of the fabricated probe, including input and output ports for frequency domain analysis, except that the aluminum fixture is not considered as it does not affect the results. The sample on the right-hand side of the probe is set to a cylinder of air (ε_r = 1), and $\varepsilon_r = 2$ is used for PTFE. The outer conductor of the coaxial probe is set to have a Perfect Electric Conductor (PEC) boundary. The E-field scale is adjusted, somewhat exaggerated, for better illustration with red indicating high E-field and blue indicating low E-field. As shown in Figure 3 (a), the sample under test interacts with the evanescent E-field at the proximity of the open-ended coaxial probe tip. This volume of interaction determines the sample size and thickness. The sample needs to be thick enough so that all available fields in the vicinity of the probe are located inside the sample under test. Practically the material thickness of four times the aperture diameter is recommended. Figure 3 (b) and (c) illustrates the electric field distribution within the coaxial probe for fundamental and fourth harmonic resonant frequencies, respectively.

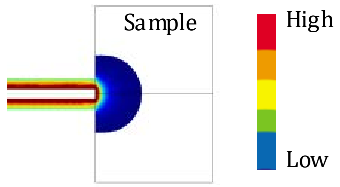

(a)

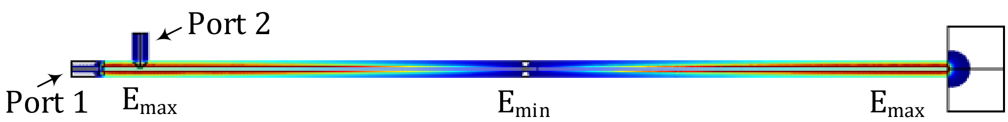

(b)

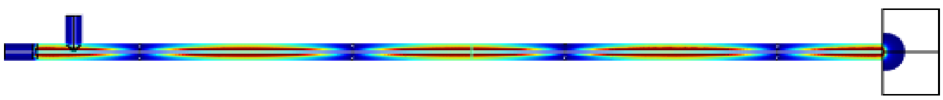

(c)

Figure 3. Full 3D simulation results modelled by using COMSOL Multiphysics. E-field distribution within the resonator and fringing field inside the sample is plotted (a) at 350 MHz (*N*=1) zoomed in to show the probe-sample boundary, (b) at 350 MHz (*N*=1), and (c) at 1400 MHz (*N*=4).

Simulated and measured broadband transmission characteristics with *air* and *water* as sample are shown in the frequency domain in Figure 4, illustrating the harmonic resonances at integer multiples of the fundamental frequency of 350 MHz. For water simulation, specific water model of H2O (Water)[liquid, distilled, 2 to 50GHz, tested at 25C (298K)] was used from COMSOL Material Library. In Figure 4 (a), the blue dotted line with empty square symbol is the COMSOL Multiphysics simulation for an air-terminated coaxial resonant probe. The black solid line with solid squares is the experimental result for the air terminated probe, showing almost perfect agreement with the simulation, and the red dashed line with solid triangle is the experimental result when the end of the probe is fully immersed in de-ionized water. The purple dotted line with empty triangle shows the simulated water response, where the discrepancy comes from the difference in material properties. All experimental data are taken using a vector network analyzer (Keysight Fieldfox N9923A). A bespoke LabVIEW program (National Instruments) is used to record and extract continuous changes in resonant frequency, 3dB (half-power) bandwidth and peak power at resonance for each resonant mode. With water as the sample under test, for each mode, the resonant frequency shifts downwards, the 3dB bandwidth increases and there is a decrease in the peak power level. We expect the amount of frequency shift and increase in 3 dB bandwidth to be proportional to the amount of water content in the sample. Figure 4 (b) shows harmonic resonant modes up to the 5th harmonic resonance.

At the frequency where the distance between the two coupling ports equates to the quarter-wavelength, in this case at 3500 MHz, the E-field minimum will be aligned with port 2 so that this mode is suppressed. This is clearly visible from the inset field distribution in Figure 4 (c), which shows broadband characteristics including 22 harmonic resonances up to 8 GHz. Since there are many modes with high quality factor available and the probe is intended to be used for tissue hydration monitoring, this missing null is not critical in investigating the broadband dielectric properties of water-based tissue samples.

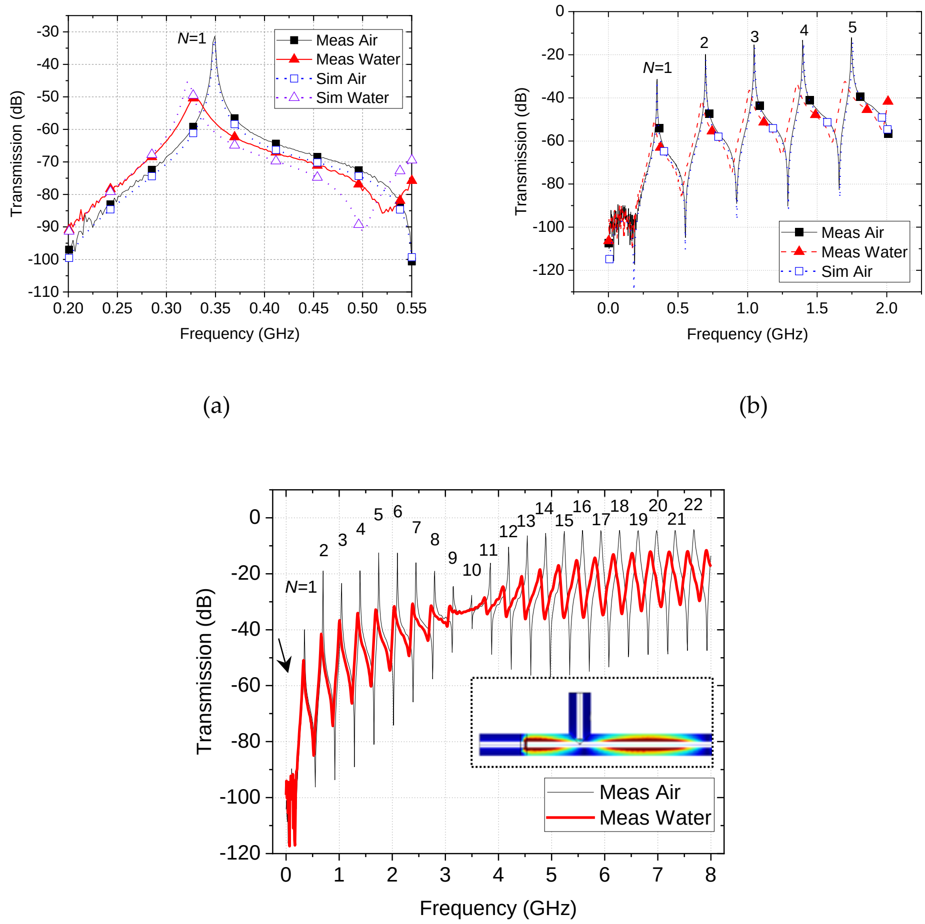

(a) (b)

(c)

Figure 4. Simulation (air) and measurement (air and water) results, (a) at the fundamental resonant frequency of 350 MHz, (b) up to 2 GHz showing 5 harmonic resonances, and (c) broadband response up to 8 GHz including 22 harmonic resonances, measured with and without water. Inset is the field distribution at 3500 MHz (*N*=10) zoomed in around the two coupling ports.

Table I summarizes the measured characteristics of the coaxial resonant probe when it is air-terminated, where each column of Frequency, f_0, Bandwidth, and Loss indicates expected harmonic resonant frequencies, measured harmonic resonant frequencies, 3 dB bandwidth, and peak insertion loss, respectively. Q_L and Q_0 indicate loaded and unloaded quality factors. The unloaded quality factor of each mode varies from a minimum of 351 to maximum of 754, allowing us to measure the change in tissue hydration level with enough fidelity.

Table 1. Measured (Air) results of the harmonic resonance coaxial probe.

Harmonic Number	Frequency (MHz)	Measured f_0 (MHz)	Bandwidth (MHz)	QL	Q0	Loss (dB)
1 *f*	350	352.6	1.0	337.5	351.1	28.3
2 *f*	700	705.3	1.6	448.9	496.0	20.5
3 *f*	1050	1058.4	2.2	488.4	569.6	16.9
4 *f*	1400	1413.3	2.8	505.1	613.8	15.0
5 *f*	1750	1766.0	3.5	503.1	624.0	14.3
6 *f*	2100	2116.9	4.2	509.3	625.8	14.6
7 *f*	2450	2471.6	5.0	495.1	592.6	15.7
8 *f*	2800	2824.5	5.7	495.6	560.6	18.7
9 *f*	3150	3182.3	7.5	425.1	451.4	24.7
10 *f*	3500	3531.3	N/A	N/A	N/A	32.1
11 *f*	3850	3883.7	8.5	455.3	507.9	19.7
12 *f*	4200	4237.5	9.5	445.0	552.0	14.3
13 *f*	4550	4590.1	11.2	411.4	560.0	11.5
14 *f*	4900	4942.9	13.5	376.2	588.0	8.9
15 *f*	5250	5297.2	13.3	397.3	679.4	7.6
16 *f*	5600	5650.5	15.0	376.3	726.4	6.3
17 *f*	5950	6002.8	16.9	355.1	754.2	5.5
18 *f*	6300	6355.8	19.9	319.9	699.5	5.3
19 *f*	6650	6707.7	23.4	286.3	692.9	4.6
20 *f*	7000	7060.8	22.6	312.3	749.6	4.7
21 *f*	7350	7413.3	24.7	299.2	732.6	4.6
22 *f*	7700	7767.4	25.5	304.3	732.0	4.7
23 *f*	8050	8122.5	30.3	268.0	583.4	5.3

3. Experiment

3.1. Sample Collection and Preparation

Human cervical samples were obtained following hysterectomies for benign gynaecological conditions not affecting the cervix at the Royal Hallamshire Hospital (Sheffield Teaching Hospitals, National Health Service Foundation Trust, U.K.). Patients gave informed written consent before the operation for use of a portion of the extirpated cervical tissue for research as approved by the North Sheffield research ethics committee (Ref-08/H1310/35) admissions procedure. Cervical samples were stored in sterile PBS supplemented with Penicillin-Streptomycin and Fungizone in 4 °C. The area of the samples varied between 2 x 2 cm^2 and 4 x 4 cm^2. Figure 5 shows an example of the cervical tissue sample. The cervical samples were 5 - 6 days old when used for experiments. For reference, anonymized batch numbers of the four tested cervical samples were sample A (030215), sample B (DT6070), sample C (WE4388), and sample D (180318).

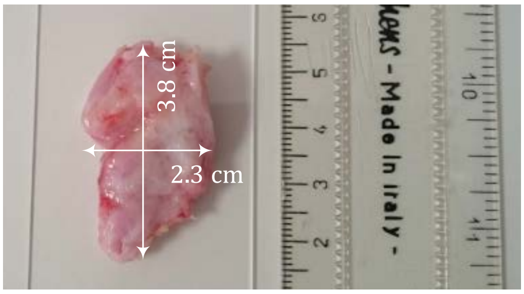

Figure 5. Cervix tissue sample with a ruler (left unit is in cm).

3.2. Experimental Setup and Test Procedure

The experimental setup consisted of the proposed resonant coaxial probe, a vector network analyzer (FieldFox, Keysight Technologies, Santa Rosa, USA) that is controlled by LabVIEW user interface on a laptop computer, and a Corneometer as a reference hydration measurement. The setup is shown in Figure 6 (a). The outer conductor of the resonant coaxial probe (copper part) was coated with Parylene (Para Tech Coating Ltd., Northampton, UK) to avoid any contamination of samples. On the day of the experiment, each sample piece was weighed immediately after removing from storage container using electronic lab micro balance. This initial weight was later referred to as 100% hydration and the samples were left to go through natural drying processes. Each sample was then weighed at every time point, before the microwave measurements were taken, and hydration level was later calculated as fraction of its initial weight. Additionally, the Corneometer (model MDD4 with CM825 probe, Courage + Khazaka electronic GmbH, Köln, Germany) was used and the moisture on the surface of the tissue was also recorded. Corneometer measurements were repeated 6 times at each time point to calculate average and standard deviation.

Each piece of cervical sample was placed on a micro balance (Pocket balance TEE, KERN & SOHN GmbH, Germany) which acted as a force sensor, as shown in Figure 6 (b). The probe was lowered and pressed against the sample with force of 5.0 ± 0.5 g. Up to the 11^{th} harmonic resonances (*N*=11, from 350 MHz to 3850 MHz) were collected except for the diminished 10^{th} harmonic component due to the reason explained previously. 15 measurements were taken at each harmonic resonance every 30 min for the duration of 3 to 48 hours (when dry or the water contents drops to below 40%) at room temperature.

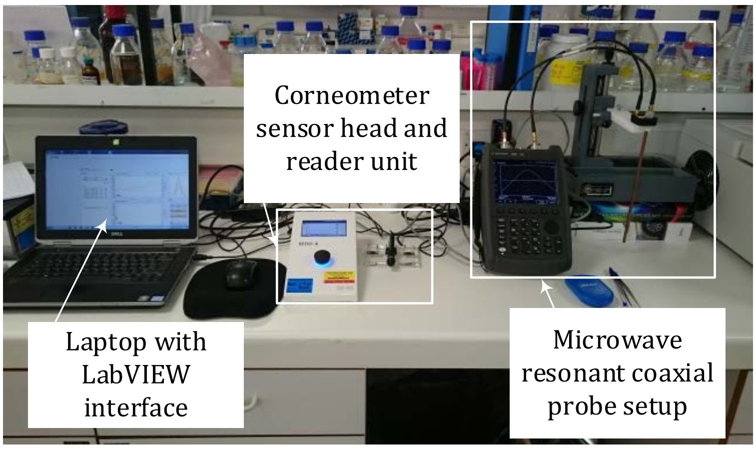

(a)

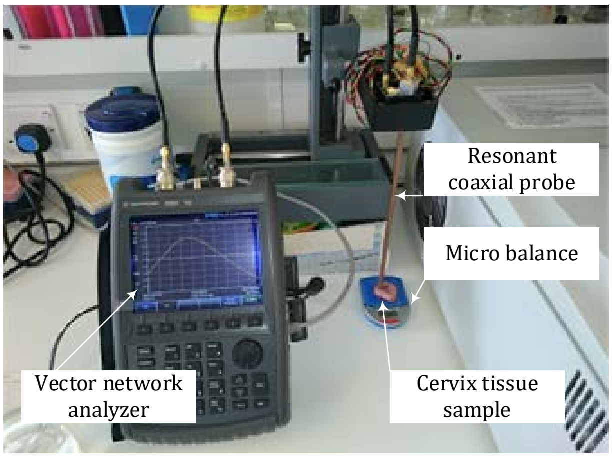

(b)

Figure 6. (a) Experimental setup, and (b) detailed resonant coaxial probe measurement setup including cervical tissue sample placed on a micro balance to monitor contact pressure.

3.2. Potential Confounders and Mitigation

There are two main types of errors, one is measurement technique-dependent, and the other is sample-dependent. As we discussed in Section II. A, one major advantage of the proposed technique is that it does not require calibration of the test instrument (e.g., vector network analyzer) because it is a 'relative' measurement technique similar to the resonant cavity perturbation method. A few of the most significant sample-dependent errors include temperature and other atmospheric conditions, probe-sample pressure including quality of probe-sample contact and sample heterogeneity [28].

3.2.1 Temperature and humidity

It is well known that the dielectric properties are temperature dependent, therefore, the room temperature was carefully monitored during the experiment. The room temperature and the humidity were controlled within 21.3±0.7 °C and 31.6±1.1 %, respectively, over the course of the experiment. Temperature dependence not only applies to the sample under test but also to the dielectric materials comprising the probe itself. In addition to this, the metallic components will also contract and expand according to the temperature, therefore affecting the resonance parameters. To characterize the temperature dependence of the fabricated resonant coaxial probe, the air-terminated probe (i.e., no sample) was placed inside an incubator (Memmert Cooled incubator, 5-70 °C) and a temperature ramp experiment was carried out over the range of 20 to 40 °C while continuously collecting the resonance parameters (f_0, bandwidth, loss, Q). To minimize the opening in the hysteresis curve due to temperature lag during a series of temperature ramp experiments, the temperature was varied from 20 °C to 40 °C and back to 20 °C over a period of 12 hours, while continuously collecting the resonance parameters. For example, through linear regression analysis between temperature and resonant frequency, a temperature coefficient of N×(26.3±1.1) kHz/ºC was obtained, where N is the harmonic number, and was used in calibrating out the temperature dependence of the probe.

3.2.2. Quality of probe-sample contact

As shown in Figure 6, the resonant coaxial probe was placed vertically on a linear stage to ensure repeatable and consistent probe-sample contact pressure. The open-end of the coaxial sensor was directly above the sample and z-axis movement was used to move the probe up and down. A piece of sample on a glass slide was placed on a micro balance to monitor the probe-tissue contact pressure, as shown in Figure 7. The probe was moved down to make a contact with a sample until the same force was applied in every contact, i.e., when the weight on display reached 5.0 ± 0.5 g, to minimize any airgap between the probe and the sample and achieve consistent quality of contact.

Figure 7. A photo showing cervix tissue-probe contact.

4. Data Analysis and Results

A basic concept of microwave perturbation in the assessment of hydration of the sample is summarized in Figure 8. The change in resonant frequency Δf and power level ΔP are calculated, referenced to the air-terminated probe, for each resonant mode. Resonator perturbation theory tells us that the fractional frequency shift, for example, is

$$\Delta f_N / f_{N,air} \approx A(\varepsilon_{\text{eff}} - 1), \quad (2)$$

where A is a dimensionless constant that depends weakly on the mode number N and ε_{eff} is the effective dielectric permittivity of the water-borne sample. In (2), Change in the amount of water in the tissue sample will affect ε_{eff}, therefore affecting the resonant frequency.

Since the permittivity of water dominates over that of the host tissue material, if the volume fraction of water is defined to be v, then we may write that $\Delta f_N / f_{N,air} \approx B + Cv$, where B and C are dimensionless constants with $B \ll C$. This allows us to infer v from simple linear regression. Similar analysis may be performed on the change in power ΔP or the change in 3dB bandwidth to determine v, but in practice the resonant frequency shift yields the most reliable and precise data.

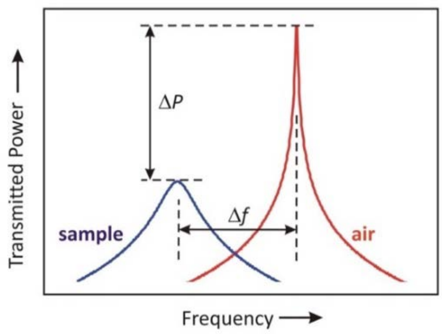

Figure 8. Microwave resonator perturbation diagram between air and sample measurement.

Figure 9 shows water content measurement of the cervical sample A (030215) over 6 hours during which the tissue dried naturally. Regarding the harmonic resonance coaxial probe, only data for the even harmonics at 700 MHz (2nd harmonic), 1400 MHz (4th harmonic) and 2100 MHz (6th harmonic) are shown in each plot but measurements are taken routinely for the first 9 modes, all showing similar trends. Fractional frequency shift is plotted since this parameter reflects the effective dielectric constant $\varepsilon_{\mathrm{eff}}$ of the sample as in equation (2), which has only a weak dependence on frequency at these low microwave frequencies, i.e., over the 1 to 2 GHz range, decreasing slightly with increasing mode number as shown in Figure 9. As it can be seen from the difference between the relative weight-based water content and the Corneometer results, the loss of water content was greater on the surface than the total water loss during the relative weight-based calculation method. This was expected because the cervical tissue does not have any protective layer, unlike skin. As the fringing electric field of the open coaxial probe has a penetration depth of only a few millimeters like the Corneometer, the Corneometer reading was used as a reference hydration level in the data analysis. The fact that the fractional frequency shift data show greater correlation with the Corneometer measurement also supports that more water is lost on the surface. Large standard deviations are observed in 6 Corneometer measurements (3 separate contacts, each contact in duplication) at each time frame as indicated by the error bar, while 15 microwave measurements show very small deviation where the error bars were too small to be visible in the plot. Also, the fluctuation of data over time is much smaller in the resonant coaxial probe. On the other hand, the dip seen at time t =150 min in the microwave measurement shows a drawback of the technique which is due to change in probe-skin contact quality such as probing location, sample inhomogeneity, or error in contact pressure control.

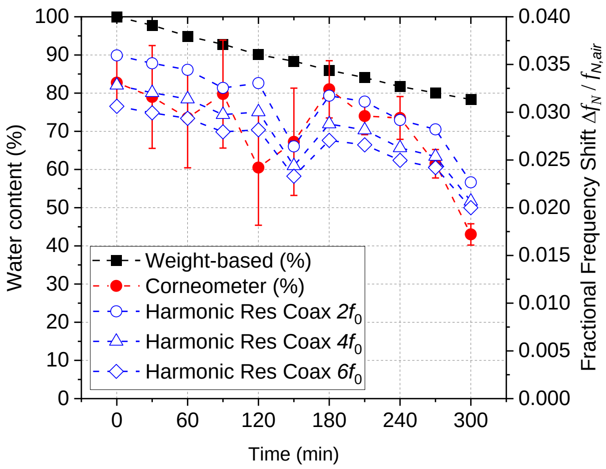

Figure 9. Water content over time of the cervix sample A (03215) measured by Corneometer (left Y-axis) and the harmonic resonance coaxial probe (right Y-axis) with relative weight-based water content (left Y-axis).

Comparison of water content of 4 different cervical samples over time and the fractional frequency shift at the 2nd harmonic frequency is shown in Figure 10. Overall, microwave resonant probe measurement shows good agreement with the Corneometer measurement, following a linear trend of losing water content over time by a natural drying process. Different samples show different rate of change due to sample-to-sample variation. It is clear that the microwave measurement produces a more linear trend than the Corneometer reading, showing less fluctuation over time, except for the sample B (DT6070) in Figure 10 (b).

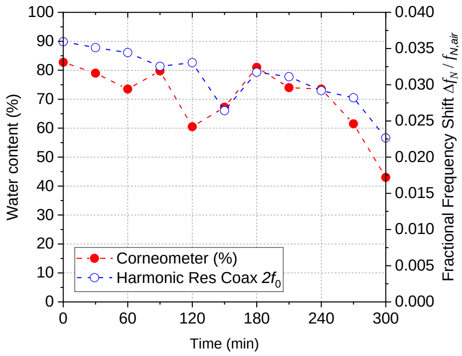

(a)

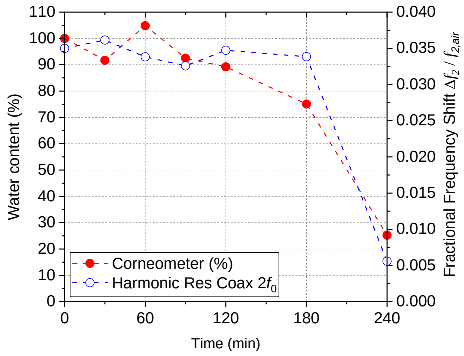

(b)

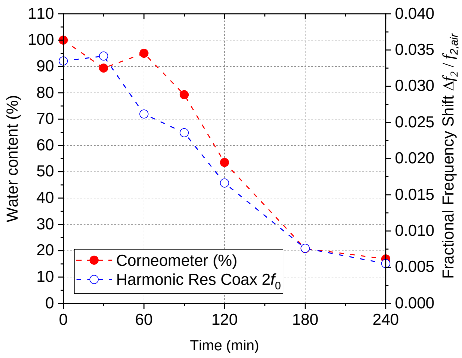

(c)

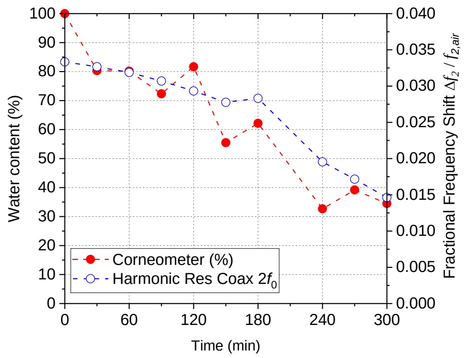

(d)

Figure 10. Water content over time measured by Corneometer and fractional frequency shift measured by the proposed harmonic resonance coaxial probe at 2nd harmonic frequency, (a) cervical sample A (030215), (b) cervical sample B (DT6070), (c) cervical sample C (WE4388), and (d) cervical sample D (180316).

All three resonant parameters (frequency, 3 dB bandwidth and peak power) are found to correlate strongly with hydration levels, with frequency chosen here as it gives the highest values of the Pearson's linear correlation coefficient, *R*. Figure 11 shows the linear correlation between Corneometer measurement and fractional frequency shift. Note the universal, linear behavior exhibited in the plots. This is to be expected, since water content, rather than tissue material, will dominate the microwave response due to its high dielectric constant. It should be noted that when the harmonic resonance coaxial probe is dipped into PBS (Phosphate-buffered saline) a fractional frequency shift of 0.038 is obtained for the 350 MHz, decreasing slightly with mode number. This is perfectly consistent with the cervix hydration data, where an average value of 0.034 ± 0.001 is found. No error bars are plotted here as it is left to the scatter in the data to indicate the error. It should be noted that the primary source of systematic error is presented by the Corneometer. Considering the non-resonant electrical impedance-based sensing mechanism of the Corneometer, the microwave resonant sensing technique is expected to be a much more accurate and error-free method of assessing hydration level. On a practical note, measurement of each mode takes less than 2 seconds, so 10 modes are measured and recorded within 20 seconds. In a final device, with bespoke and optimized electronics, it is expected that only three modes would need to be measured for reliable hydration levels to be determined, and for the measurement and data recording to be completed within only 2 seconds.

In terms of sensitivity, the proposed sensor shows mean fractional frequency shift of (3.3±0.3)*10^{-4} per unit % over the entire data collected (e.g., 4 different samples and 3 harmonic resonances). This translates into an absolute frequency shift (Δf_N) of 252±23 kHz/%, 455±41 kHz/%, and 647±57 kHz/% at 2nd, 4th, and 6th harmonic resonance, respectively.

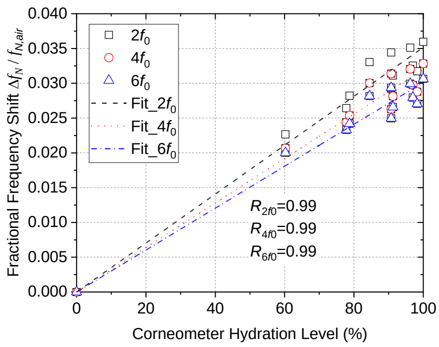

(a)

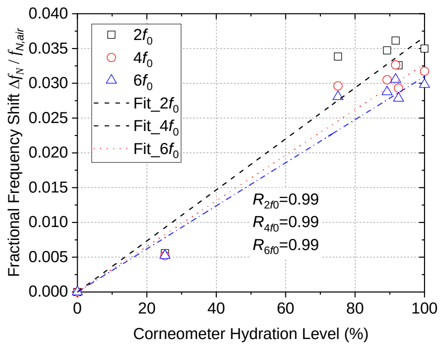

(b)

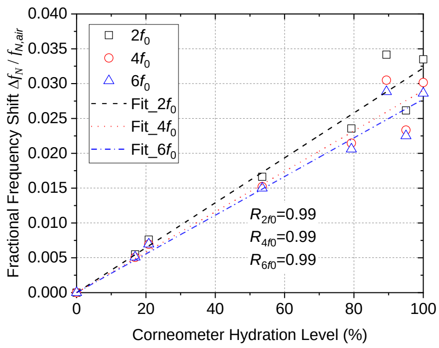

(c)

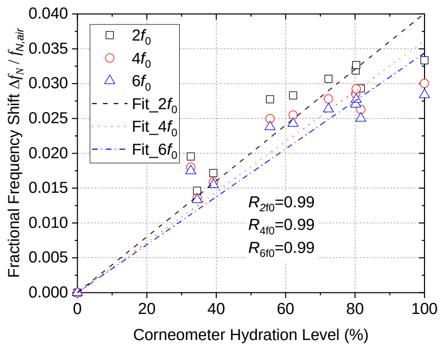

(d)

Figure 11. Correlation between Corneometer reading and fractional frequency shift data of the first three even harmonic resonances, (a) cervical sample A (030215), (b) cervical sample B (DT6070), (c) cervical sample C (WE4388), (d) cervical sample D (180316).

5. Conclusions

A microwave resonant open coaxial probe sensor with harmonic resonances was designed for non-invasive human cervical tissue hydration level monitoring. Estimated hydration level measured by the proposed resonant open coaxial probe shows high and linear correlation compared with the data collected by a commercial skin hydration sensor. This was expected from the fact that water has high dielectric constant and there will be high dielectric contrast as the water content changes in the cervical tissue samples. From a series of *in vitro* experiments on human cervix tissue samples, we can conclude that the proposed probe has been shown to have high accuracy and good precision thanks to its resonant characteristic with high Q factor.

As discussed in Section 3.2, tight monitoring and control of error sources is the key in obtaining reliable, repeatable, and clinically meaningful data. Further *in vivo* study would require design modifications and relevant ethical approval process. Finally, we note that a probe of this sort, based on RG401 coaxial cable and enclosed in a suitable polymer casing, would be a convenient geometry for such non-invasive *in vivo* testing and form the basis of a medical diagnostic device.

Author Contributions: "Conceptualization, A.P., A.A., H.C., and D.A.; methodology, A.P., D.A., E.B.; software, H.C.; validation, E.B., A.A., A.P., H.C. and D.A.; formal analysis, E.B., A.P., and H.C.; data curation, E.B., A.P., and H.C.; writing—original draft preparation, H.C., A.P. and E.B.; writing—review and editing, H.C., A.P., E.B., A.A. and D.A.; visualization, H.C. and A.P; supervision, A.P. and D.A.; funding acquisition, A.P. and D.A. All authors have read and agreed to the published version of the manuscript."

Funding: "This research was funded by a University of Sheffield Medical Research Council Confidence in Concept Knowledge Exchange Grant awarded to D.A. and A.P.

Institutional Review Board Statement: "The study was conducted in accordance with the Declaration of Helsinki, and approved by the the North Sheffield research ethics committee (Ref-08/H1310/35) (Protocol version 2 date 30 April 2008) for studies involving humans.

Informed Consent Statement: "Informed consent was obtained from all subjects involved in the study."

Data Availability Statement: "Not applicable".

Acknowledgments: "Not applicable".

Conflicts of Interest: "The authors declare no conflict of interest."

Appendix A

Fractional frequency shift data can be converted into a relative hydration level (%) either by simply normalizing a selected harmonic resonance to the base-line fractional frequency shift value at time t =0, i.e., when the sample was taken out of suspension liquid, as 100% hydration, or by finding a linear fit equation. Figure A1 shows the comparison of Corneometer reading and the proposed harmonic resonance coaxial probe measurements for sample A. For fair comparison, all the Corneometer readings were offset by 17.3% so the reading at time t=0 matches 100%. Pearson's linear correlation coefficient for both measurements seem to be similar while microwave technique shows a little bit more correlation (0.97 compared with 0.92). However, the mean square error (MSE) is much smaller for the microwave technique, showing half the value of the Corneometer measurements (42 compared with 84), which is also clearly indicated as the grouping in a smaller area in the Regular Residual plot shown in Figure A1 (b).

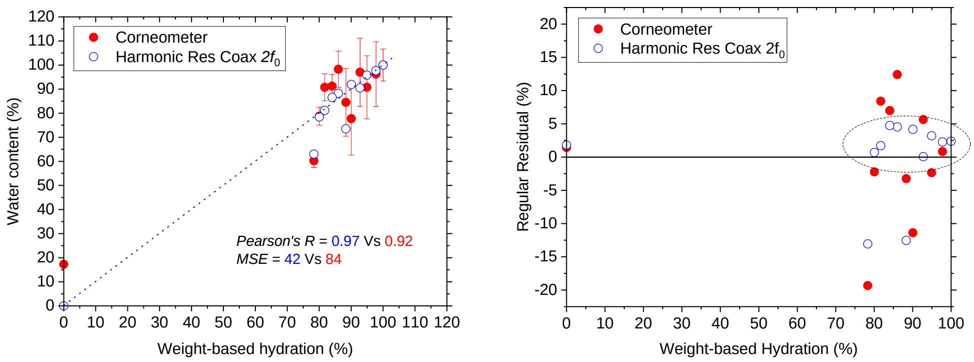

(a) (b)

Figure A1. Accuracy comparison of Corneometer and the harmonic resonant coaxial probe with respect to weight-based water content for sample A. (a) correlation chart, and (b) regular residual data after linear fit.

References

1. World Health Organization, 'Preterm birth', 2018. [Online]. Available: https://www.who.int/news-room/fact-sheets/detail/preterm-birth. [Accessed: 18-May-2022].
2. World Health Organization, 'Systematic review on maternal mortality and morbidity: the global burden of preterm birth', *Bull World Health Organ.*, vol. 88, no. 1, pp. 31–38, Jan. 2010.
3. Centers for Disease Control and Prevention, 'Preterm Birth', 2021. [Online]. Available:
4. https://www.cdc.gov/reproductivehealth/maternalinfanthealth/pretermbirth.htm. [Accessed: 18-May-2022].
5. S. O'Hara, M. Zelesco and Z. Sun, "Cervical length for predicting preterm birth and a comparison of ultrasonic measurement techniques", *Australas J. Ultrasound Med*., vol. 16, no. 3, pp. 124-134, Aug. 2013.
6. H. Feltovich, T. J. Hall and V. Berghella, "Beyond cervical length: emerging technologies for assessing the pregnant cervix", *Am. J. Obstet. Gynecol*., vol. 207, no. 5, pp. 345-354, Nov. 2012.
7. H. Feltovich and L. Drehfal, "New techniques in evaluation of the cervix", *Semin Perinatol*., vol. 41, no. 8, pp. 477-484, Dec. 2017.
8. D. A. Schoeller, "Isotope tracers in metabolic research: Principles and practice of kinetic analysis*", The Quarterly Review of Biology*, vol. 82, no. 1, pp. 43-44, Mar. 2017.
9. A. Thomasset, "Bioelectrical properties of tissue impedance", *Lyon Medical*, vol. 207, pp. 107-118, 1962.
10. T. J. Faes, H. A. van der Meij, J. C. de Munck, R. M. Heethaar, "The electrical resistivity of human tissues (100 Hz – 10 MHz): a meta-analysis of review studies", *Physiol. Meas*., vol. 20, no. 4, pp. R1 – R10, May 1999.
11. J. B. Matthie, *et al.,* "Analytic assessment of the various bioimpedance methods used to estimate body water", *J. Appl. Physiol.,* vol. 84, no. 5, pp. 1801-1816, May 1998.
12. M. D. Vanloan and P. D. Mayclyn, "A new TOBEC instrument and procedure for the assessment of body composition: the use of Fourier coefficients to predict lean body mass and total body water", *Am. J. Clin. Nutr.* vol. 45, pp. 131-137, 1987.
13. A. D. Lorenzo and A. Andreoli, "Segmental bioelectrical impedance analysis", *Curr. Opin. Clin. Nutr. Metab. Care*, vol. 6, no. 5, pp. 551-556, 2003.
14. J. A. Jackobson, "Musculoskeletal sonography and MR imaging: A role for both imaging methods", *Radiol. Clin. North Am.*, vol. 37, no. 4, pp. 713-35, 1999.
15. P. Peetrons, "Ultrasound of muscles", *Eur. Radiol.*, vol. 12, no. 1, pp. 35-43, 2002.
16. F. Schick, "Pulsed magnetization transfer contrast MRI by a sequence with water selective excitation", *J. Comput. Assist. Tomogr.*, vol. 20, no. 1, pp. 73-79, 1996.
17. B. M. de Tejada, *et al.,* "Magnetic resonance imaging of the cervix in women at high risk for preterm delivery", J. Matern. Fetal Neonatal Med., vol. 24, no. 11, pp. 1392-1397, Nov. 2011.
18. J. T. Keeton, *et al.*, "Rapid determination of moisture and fat in meats by microwave and nuclear magnetic resonance analysis", *PVM 1: 2003, J.AOAC Int.*, vol. 86, no. 6, pp. 1193-1202, 2003.
19. X. Xu and R. K. Wang, "The role of water desorption on optical clearing of biotissue: studied with near infrared reflectance spectroscopy", *Med. Phys.* Vol. 30, no. 6, pp. 1246-1253, 2003.
20. R. J. Kuon, *et al*., "A novel optical method to assess cervical changes during pregnancy and use to evaluate the effects of progestins on term and preterm labor", Am. J. Obstet. Gynecol. vol. 205, no. 1, pp. 82.e15–82.e20, Feb. 2011.
21. M. P. O'Connell, *et al.*, "An in vivo comparative study of the pregnant and nonpregnant cervix using electrical impedance measurements", British J. Obstet. Gynecol., vol. 107, no. 8, pp. 1040–1041, Aug. 2000.
22. B. L. McFarlin, *et al.*, "Ultrasonic attenuation estimation of the pregnant cervix: a preliminary report", Ultrasound Obstet. Gynecol., vol. 36, no. 2, pp. 218-225, Aug. 2010.
23. C. M. O'Brien, *et al.*, "Raman spectroscopy provides a noninvasive approach for determining biochemical composition of the pregnant cervix in vivo", vol. 103, no. 7, pp. 715-721, Jul. 2014.
24. H. Scharfetter, R. Casanas and J. Rosell, "Biological tissue characterization by magnetic induction spectroscopy (MIS): Requirements and limitations", IEEE Trans. Biomed. Engineering, vol. 50, no. 7, pp. 870-880, Jul. 2003.
25. J. -Y Wang, *et al.,* "Magnetic induction spectroscopy (MIS) – probe design for cervical tissue measurements", Physiol. Meas., vol. 38, no. 5, pp. 729-742, Apr. 2017.
26. S. F. A. Halim, *et al*., "A review on magnetic induction spectroscopy potential for fetal acidosis examination", vol. 22, no. 1334, pp. 1 – 36, Feb. 2022.
27. R. Wickett, "Hardware and measuring principles: the Nova Dermal Phase Meter", *In Bioengineering of the Skin. Water and the Stratum Corneum (Fluhr J., Elsner P., Berardesca E., Maibach HI. Eds.*) Boca Raton, FL, CRC Press, pp. 263-274, 2005.
28. "Corneometer® CM 825," courage-khazaka.de https://www.courage-khazaka.de/en/16-wissenschaftliche-produkte/alle-produkte/183-corneometer-e (accessed: May. 19, 2022).

29. A. La Gioia, E. Porter, I. Merunka, A. Shahzad, S. Salahuddin, M. Jones, and M. O'Halloran, "Open-Ended Coaxial Probe Technique for Dielectric Measurement of Biological Tissues: Challenges and Common Practices," *Diagnostics*, vol. 8, no. 2, p. 40, Jun. 2018.
30. Stuchly, M.A.; Athey, T.W.; Samaras, G.M.; Taylor, G.E. Measurement of Radio Frequency Permittivity of Biological Tissues with an Open-Ended Coaxial Line: Part II—Experimental Results. IEEE Trans. Microw. Theory Tech. 1982, 30, 87–92.
31. Burdette, E.; Cain, F.; Seals, J. In Vivo Probe Measurement Technique for Determining Dielectric Properties at VHF through Microwave Frequencies. IEEE Trans. Microw. Theory Tech. 1980, 28, 414–427.
32. Kraszewski, A.; Stuchly, M.A.; Stuchly, S.S.; Smith, A.M. In Vivo and in Vitro Dielectric Properties of Animal Tissues at Radio Frequencies. Bioelectromagnetics 1982, 3, 421–432.
33. Gabriel, S.; Lau, R.W.; Gabriel, C. The Dielectric Properties of Biological Tissues: II. Measurements in the Frequency Range 10 Hz to 20 GHz. Phys. Med. Biol. 1996, 41, 2251–2269.
34. Gabriel, S.; Lau, R.W.; Gabriel, C. The Dielectric Properties of Biological Tissues: III. Parametric Models for the Dielectric Spectrum of Tissues. Phys. Med. Biol. 1996, 41, 2271–2293.
35. Peyman, A.; Holden, S.; Gabriel, C. Mobile Telecommunications and Health Research Programme: Dielectric Properties of Tissues at Microwave Frequencies; Microwave Consultants Limited: London, UK, 2005.
36. Abdilla, L.; Sammut, C.; Mangion, L. Dielectric Properties of Muscle and Liver from 500 MHz–40 GHz. Electromagn. Biol. Med. 2013, 32, 244–252.
37. Schwan, H.P.; Foster, K.R. RF Field Interactions with Biological Systems: Electrical Properties and Biophysical Mechanisms. Proc. IEEE 1980, 68, 104–113.
38. Gregory, A.; Clarke, R.; Hodgetts, T.; Symm, G. RF and Microwave Dielectric Measurements upon Layered Materials Using Coaxial Sensors; NPL Report MAT 13; National Physical Laboratory: Teddington, UK, 2008.
39. Keysight Technologies, *Basics of measuring the dielectric properties of materials,* Appl. Note 5989-2589EN, pp. 1-35.
40. D. M. Pozar, Microwave Engineering, 3rd ed. New York: Wiley, 2005.
41. O'Rourke, A.P.; Lazebnik, M.; Bertram, J.M.; Converse, M.C.; Hagness, S.C.; Webster, J.G.; Mahvi, D.M. Dielectric Properties of Human Normal, Malignant and Cirrhotic Liver Tissue: In Vivo and Ex Vivo Measurements from 0.5 to 20 GHz Using a Precision Open-Ended Coaxial Probe. Phys. Med. Biol. 2007, 52, 4707–4719.
42. Athey, T.W.; Stuchly, M.A.; Stuchly, S.S. Measurement of Radio Frequency Permittivity of Biological Tissues with an Open-Ended Coaxial Line: Part I. IEEE Trans. Microw. Theory Tech. 1982, 30, 82–86.
43. Stuchly, M.A.; Stuchly, S.S. Coaxial Line Reflection Methods for Measuring Dielectric Properties of Biological Substances at Radio and Microwave Frequencies-A Review. IEEE Trans. Instrum. Meas. 1980, 29, 176–183.
44. Athey, T.W.; Stuchly, M.A.; Stuchly, S.S. Measurement of Radio Frequency Permittivity of Biological Tissues with an Open-Ended Coaxial Line: Part I. IEEE Trans. Microw. Theory Tech. 1982, 30, 82–86.
45. Gabriel, C.; Grant, E.H.; Young, I.R. Use of Time Domain Spectroscopy for Measuring Dielectric Properties with a Coaxial Probe. J. Phys. E 1986, 19, 843–846.
46. Alanen, E.; Lahtinen, T.; Nuutinen, J. Variational Formulation of Open-Ended Coaxial Line in Contact with Layered Biological Medium. IEEE Trans. Biomed. Eng. 1998, 45, 1241–1248.
47. Hagl, D.; Popovic, D.; Hagness, S.C.; Booske, J.H.; Okoniewski, M. Sensing Volume of Open-Ended Coaxial Probes for Dielectric Characterization of Breast Tissue at Microwave Frequencies. IEEE Trans. Microw. Theory Tech. 2003, 51, 1194–1206.
48. Popovic, D.; Okoniewski, M.; Hagl, D.; Booske, J.H.; Hagness, S.C. Volume Sensing Properties of Open Ended Coaxial Probes for Dielectric Spectroscopy of Breast Tissue. In Proceedings of the IEEE Antennas and Propagation Society, Boston, MA, USA, 8–13 July 2001; pp. 254–257.
49. Popovic, D.; McCartney, L.; Beasley, C.; Lazebnik, M.; Okoniewski, M.; Hagness, S.C.; Booske, J.H. Precision Open-Ended Coaxial Probes for in Vivo and Ex Vivo Dielectric Spectroscopy of Biological Tissues at Microwave Frequencies. IEEE Trans. Microw. Theory Tech. 2005, 53, 1713–1721.
50. A. Fallahi, S. Hashemizadeh and N. Kuster, "On the Dielectric Measurement of Thin Layers Using Open-Ended Coaxial Probes," in IEEE Transactions on Instrumentation and Measurement, vol. 70, pp. 1-8, 2021, Art no. 6011808.
51. Jingchen Wang, Eng Gee Lim, Mark Paul Leach, Zhao Wang, Ka Lok Man, "Open-Ended Coaxial Cable Selection for Measurement of Liquid Dielectric Properties via the Reflection Method", Mathematical Problems in Engineering, vol. 2020, Article ID 8942096, 8 pages, 2020.
52. M. Shao et al., "Time Domain Calibration Method of Open-Ended Coaxial Probe in Dielectric Measurement," in IEEE Transactions on Instrumentation and Measurement, vol. 71, pp. 1-8, 2022, Art no. 9503308.
53. I. Dilman, M. N. Akinci, T. Yilmaz, M. Çayören and I. Akduman, "A Method to Measure Complex Dielectric Permittivity With Open-Ended Coaxial Probes," in IEEE Transactions on Instrumentation and Measurement, vol. 71, pp. 1-7, 2022, Art no. 6000507, doi: 10.1109/TIM.2022.3147878.
54. D. J. Rowe, J. Naylon, A. Porch, D. A. Barrow, and C. J. Allender, "Microwave resonant sensor for real-time continuous-flow measurements of microfluidic systems," in *Proc. 15th Int. Conf. Miniaturized Syst. Chemistry and Life Sci.*, Groningen, Germany, 2010, pp. 1004-1006.
55. D. J. Rowe, A. Porch, D. A. Barrow, and C. J. Allender, "Integrated microwave resonant device for dielectric analysis of microfluidic systems," in *J. Physics: Conf. Series,* Aug. 2011, vol. 310, Art. ID 012004.

56. D. J. Rowe, A. Porch, D. A. Barrow, and C. J. Allender, "Dielectric analysis of microfluidic systems with an integrated microwave resonant device," in *Proc. 41st Eur. Microw. Conf.*, Manchester, U.K., 2011, pp. 607-610.
57. D. J. Rowe, A. Porch, D. A. Barrow, and C. J. Allender, "Non-contact label-free dielectric spectroscopy of single-and multi-phase microfluidic systems," in *Proc. 16th Int. Conf. Miniaturized Syst. Chemistry and Life Sci.*, Seattle, WA, 2011, pp. 891-893.
58. D. J. Rowe, A. Porch, D. A. Barrow, and C. J. Allender, "Novel coupling structure for the resonant coaxial probe," *IEEE Trans. Microw. Theory Tech.*, vol. 60, no. 6, pp. 1699-1708, Jun. 2012.
59. D. J. Rowe, A. Porch, D. A. Barrow, and C. J. Allender, "Microfluidic device for compositional analysis of solvent systems at microwave frequencies," *Sens. Actuators B, Chem.*, vol. 169, pp. 213-221, July 2012.
60. D. J. Rowe, A. Porch, D. A. Barrow, and C. J. Allender, "Microfluidic microwave sensor for simultaneous dielectric and magnetic characterization," *IEEE Trans. Microw. Theory Tech.*, vol. 61, no. 1, pp. 234-243, Jan. 2013.
61. D. K. Misra, "Quasi-static analysis of open-ended coaxial lines," IEEE Trans. Microw. Theory Tech., vol. 35, no. 10, pp. 925–928, Oct. 1987.
62. C. Gabriel, T. Y. A. Chan, and E. H. Grant, "Admittance models for open ended coaxial probes and their place in dielectric spectroscopy," Phys. Med. Biol., vol. 39, no. 12, pp. 2183–2200, Dec. 1994.
63. J.-H. Kim, B. Enkhbayar, J.-H. Bang, B.-C. Ahn, and E.-J. Cha, "New formula for the reflection coefficient of an open-ended rectangular waveguide with or without an infinite flange," Progr. Electromagn. Res. M, vol. 12, pp. 143–153, 2010.